Regulative Characteristic of Methanol–Copper Heat Pipes for Asteroid Lander "MASCOT"

Volodymyr Baturkin[1*], Vitali Feidelheimer[2], Kaname Sasaki[1], Eugen Mikulz[1] and Tra-Mi Ho[1]

[1]*DLR – Institute of space systems, Bremen, 28359, Germany*
[2]*FH Aachen – University of Applied Sciences, Aachen, 52064, Germany*

Abstract

Variable conductance heat pipes (VCHPs) are the main part of MASCOT (Mobile Asteroid surface SCOuT) lander thermal control system (TCS). They provide variable conductivity by utilizing the heat transfer limitations. This allows the heat pipes to act as thermal switches without additional constructive elements. The advantage is simplicity and compactness of conventional heat pipe design. Two cylindrical copper-methanol heat pipes with shell length of 0.482 m and 0.438 m and external diameter of 0.006 m, having copper discrete metal fiber wick and copper shell were constructed and verified in the temperature range between −75 and +60 °C. The purpose is to apply this design into the MASCOT thermal control system and to investigate their regulative characteristics and heat transfer limitations. VCHPs show a change of thermal resistivity from 70 K/W, at a heat sink temperature of −60 °C, to 0.8 K/W at a heat sink temperature of +60 °C; with a obtained maximal heat transfer rate of 5 W and 16 W, respectively. It is found, that the switching effect of the heat pipes is governed by the sonic velocity limitation, the saturation vapor pressure of the working fluid and the maximal capillary pressure of the wick. Operation of heat pipes as the part of TCS has confirmed their variable thermal properties.

Keywords: Heat transfer limitations; Variable conductance; Metal fiber wick; Space application; Methanol-Copper.

1. INTRODUCTION

Since the launch on December 3rd 2014, the Hayabusa2 (HY2) spacecraft and the onboard compact landing package MASCOT (Mobile Asteroid surface SCOuT) is on their way to Near Earth asteroid (162173) Ryugu [1]. After the arrival at asteroid Ryugu in June/July 2018, MASCOT will be separated to perform in-situ investigation of the asteroid with its four science instruments: a camera 'MASCAM' [2], a near-IR hyperspectral microscope 'MicrOmega' [3], a magnetometer 'MASMAG' [4] and a radiometer 'MARA' [5].

MASCOT Thermal Control System (TCS) has to assure that all subsystems and payloads are in dedicated temperature ranges over the mission lifetime. This is realized by a delicate design of thermal interfaces between different components [6], and one of the most important interfaces is the connection between an electronic box and a radiator. MASCOT main components, thermal interfaces, and heater locations are described in Fig. 1. A major challenge of MASCOT TCS design is to satisfy diverse thermal requirements in different mission phases. While HY2 is in a cruise phase and an asteroid proximity operation, MASCOT power is nominally off, except for some MASCOT flight operations, and only survival heaters are powered by HY2. Regarding the thermal environment, MASCOT is shadowed by the HY2 high gain antenna. As an interface requirement, considering the possible conductive and radiative interface temperature variation −20…+60 °C, heat exchange between MASCOT and HY2 has to be within ±5 W. During this phase, MASCOT subsystems and payloads have to stay within their non-operational temperature limits, and one of the most temperature sensitive equipment is a battery pack, the temperature of which has to be maintained around −30 °C.

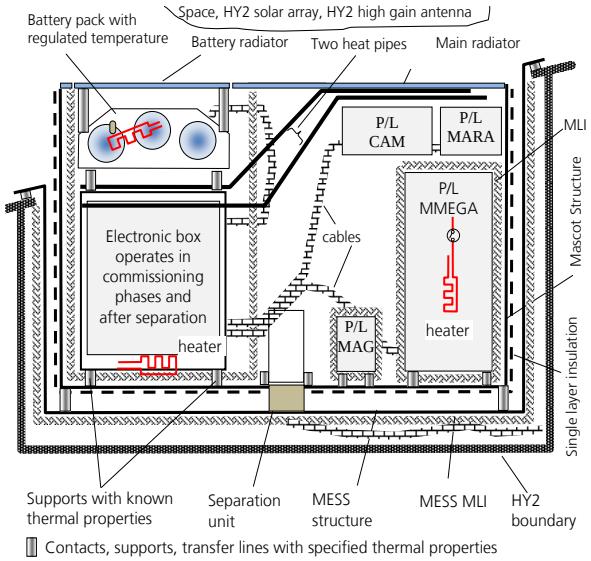

Fig. 1. Main components of MASCOT lander and component of TCS. MESS structure is used for attachment of lander to HY2 and it stays as a part of HY2 after the lander separation. Surfaces with specified optical properties, external cables, some equipment are not shown

At periodic MASCOT operations, such as health checks and payload calibrations, TCS shall provide corresponding operational temperatures for subsystems and payloads. Before every MASCOT turn on, dedicated MASCOT pre-heating operation, which is realized by a setting change of the survival heaters, is performed. Considering these phases, MASCOT TCS should limit the heat exchange with HY2 and with the environment, in order to satisfy the interface requirement and to use the survival heaters efficiently.

Contrary to the cruise phase and the asteroid proximity operation, MASCOT is subject to a dynamic thermal environment during the on-asteroid operation. In order to deliver MASCOT to the asteroid surface, HY2 will first descend from its home position at 20 km towards the asteroid. During this phase, MASCOT will receive increasing thermal radiation from the asteroid. Afterwards, MASCOT is separated from HY2, starts freefall to the asteroid surface, and bounces on the surface until it reaches a settled condition. In this phase, heat fluxes from the sun and the asteroid flow into MASCOT sides. On the asteroid surface, MASCOT experiences large variations of the solar flux and the asteroid surface temperature, because of the day and night transition of the asteroid. Under this dynamic thermal environment, MASCOT performs intensive payload operations. Therefore, during the on-asteroid phase, MASCOT TCS has to efficiently reject the generated heat through the radiator.

After a trade-off study of the MASCOT TCS design, a specific type of heat pipe was selected as a heat transfer component between the electronic box and the radiator. This type of heat pipes has an external shape of constant conductance heat pipes, but a thermal performance is similar to that of variable conductance heat pipes [7]. They were developed and fabricated by the National Technical University of Ukraine "Kyiv Polytechnic Institute". Such type of heat pipes has the flight heritage in projects SKALA (1980), Fragment (1983) and Magion-4&5 (1995, 1996) [8]. Developed heat pipes operated at heat sink temperature −10 …+50 °C) and transferred heat power (2…20 W). Minimal/maximal thermal resistance makes 1.2 K/W to 8 K/W.

The mechanism of variable heat transfer in methanol-copper heat pipes is connected with dramatic variation of heat carrier thermophysical properties, which impose the heat pipes in different regimes of operation. In some regimes the heat pipes operate in conditions with limited circulation of vapour and liquid between condenser and evaporation. Such conditions in heat pipe practice are considered to be not desirable. In this paper the peculiarities of methanol-copper heat pipe operation is considered in more details, concentrating the attention on their variable thermal properties.

Two methanol-copper heat pipes with a sintered metal fiber wick are examined in this study. They are the two-dimensional versions of the three-dimensional heat pipes integrated in MASCOT. The heat pipe type A (HP-A) has four curvatures (2 × 90° and 2 × 120°) and the heat pipe type B (HP-B) has five curvatures (2 × 24° and 3 × 90°), as shown in Fig. 2 and Table 1. The important direction of this study is to understand the heat transfer limitations effect on the variable characteristics of this type of heat pipes.

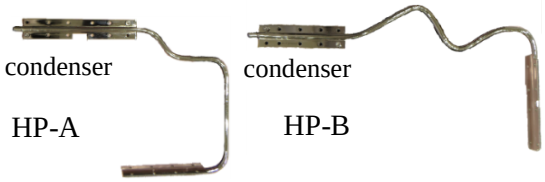

Fig. 2. Configuration of 2D heat pipes, HP-A and HP-B used in current research.

Table 1. Characteristics of investigated heat pipes.

Property	HP-A	HP-B
Working fluid	Methanol	
Material / Wick	Copper	
Wick type	Metal fiber	
d_s	6mm	
d_v	3.1mm	
d_w	5mm	
K	$9.36\times10^{-10}m^2$	
E	0.82 to 0.84	
V_{wf}	6ml	5ml
L_A	259mm	256mm
L_C	127mm	83mm
L_E	96mm	99mm
L_{Eff}	370.5mm	347mm
L_T	482mm	438mm
m_{HP}	0.123kg	0.112kg

2. LIMITING FACTORS OF HEAT TRANSFER

The investigated methanol-copper heat pipes are designed to operate in a temperature range between −80 °C and 120 °C. In this range, they are subject to several heat transfer limitations. During the design of a heat pipe, the calculation and the knowledge of the occurrence of limitations are essential. For conventional design, it is the primary objective to avoid an operation in the limiting regime, to guarantee the best performance. Faghri [10] has summarized the occurrence of heat trans-

*Corresponding author: volodymyr.baturkin@dlr.de, Phone: +49 (0) 421-24420-1610

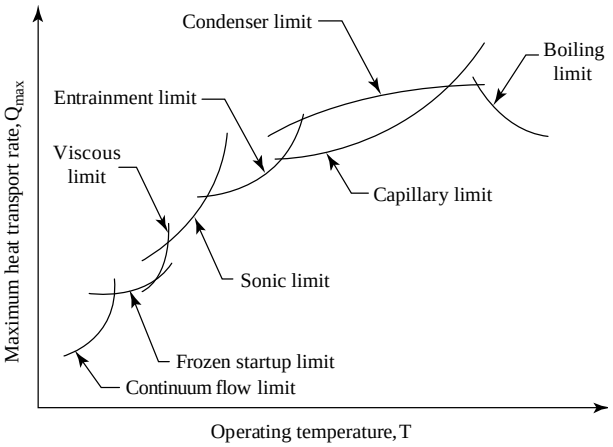

Fig. 3. Heat transfer limitations of heat pipes at different operating temperatures [10].

fer limitations as a function of the operating temperature (or saturation pressure / temperature) and the heat input. Fig. 3 shows this relation qualitatively, indicating that the limitations have transition zones where they interact together. However, in the analytical calculation they are treated individually with no perturbations and are only valid for steady state in the operating domain. This domain is below the line of any limitation which may be encounter first. But, heat pipes operating above the calculated limitations are subject to a more complicated state. The nearly isothermal behavior of a heat pipe does not exist anymore and a definition of an operating temperature is not straightforward. A temperature difference between evaporator and condenser can be more than 100 °C. From the analytical calculation it is impossible to identify the acting limitation, or a combination of them. However, exactly this behavior is desired by a VCHP. It separates the cold heat sink with the hot operating payload. The identification of the heat transfer limitations that cause the variable conductance of the methanol-copper heat pipes with fibrous capillary structure is the primary objective.

For the calculation of the heat transfer limitations is developed a custom-made methanol thermophysical properties database. This is required since there is no reference with all required thermophysical properties. Especially for temperatures below -40 °C, the properties spread up to 20% between the used sources. These properties are calculated by the temperature ratio $T_\mathrm{r} = T/T_\mathrm{C}$, where the critical temperature T_C = 512.5 K, and the temperature of interest T. The polynomial is defined by

$$f(T) = \sum_{i=0}^{1\ldots3} A_i \cdot T_\mathrm{r}^i, \qquad (1)$$

Table 2. Coefficients of thermophysical properties of methanol calculated with Eqn. 1 given in SI units.

Property	A_0	$A_1 T_\mathrm{r}$	$A_2 T_\mathrm{r}^2$	$A_3 T_\mathrm{r}^3$
λ_l	0,300823	-0,176481	0	0
λ_v	-0,012552	0,112281	-0,205586	0,161913
ρ_l	1069,444	-486,028	0	0
$10^6 \mu_\mathrm{v}$	-0,294716	17,11866	0	0
$10^{-6} H_\mathrm{fg}$	1,710327	-2,163057	3,979509	-3,192026
σ	0,055371	-0,066307	0,017467	0
Property	A_0	$A_1 T_\mathrm{r}^{-1}$	$A_2 T_\mathrm{r}^{-2}$	$A_3 T_\mathrm{r}^{-3}$
$\ln(\rho_\mathrm{v})$	11,44934	-6,593777	-0,550823	0
$\ln(\mu_\mathrm{l})$	-12,15963	2,868341	-0,095127	0
$\ln(p_\mathrm{sat})$	-23,94323	-7,513269	-0,43977	0

where $f(T)$ is the searched property in SI units and A_i is a coefficient of the polynomial. The coefficients are given in Table 2 with validity between −80 and 150 °C. Subscript l is used for liquid and v for vapor.

From the shown heat transfer limitations in Fig 3, the following limitations can be excluded. (1) the continuum flow limitation is only of concern for vapor flow in the rarefied condition. Investigation of the Knudsen number for this heat pipes shows a maximal Knudsen number of $Kn_\mathrm{max} = 0.23$ at a saturation temperature of −80 °C, which is in the region of slip flow. The heat pipes are therefore at no point in rarefied flow conditions. Continuum flow condition is fully established at a saturation temperature of −51 °C ($Kn = 0.01$). (2) the frozen start up limitation is a subject of high temperature heat pipes starting from frozen state. The used working fluid methanol has a melting point at −97.6 °C, which is below the operational temperature. (3) the condenser limitation is reached when the heat sink is not able to reject the applied heat. In this investigation, this is at no point the case. The heat rejection rate is higher than the applied heat. Further, this limitation can only be reached when all other are not encountered, which is never the case for this heat pipes. (4) even though the heat pipes operate above the boiling point of methanol (64.7 °C), the boiling limitation for heat pipes with metal fiber wicks is not a limiting factor but the fundamental operational mode as pointed out by Semena [11].

The remaining limitations are the viscous, sonic, entrainment and capillary limitation. The viscous and sonic limitations are connected to the vapor flow and low saturation temperatures. The capillary limitation is mainly connected with the liquid flow. The entrainment limitation is a function of the vapor flow velocity and the surface tension of the liquid phase. These four limitations are described in more detail below.

In the viscous limitation, the heat pipes operate near the triple point with low saturation pressure. The heat transfer is limited because of the viscous forces of the vapor flow and the limited maximal possible pressure drop. Busse [12] made an analytical approach to find the viscous limitation. Taking the assumption of a laminar and isothermal perfect gas, the limitation can be described by

$$Q_{\mathrm{v,max}} = \frac{A_\mathrm{v} d_\mathrm{v}^2 H_\mathrm{fg} \rho_0 p_0}{64 \mu_\mathrm{v} L_\mathrm{Eff}} \left(1 - \frac{p_{\mathrm{L_T}}^2}{p_0^2}\right). \quad (2)$$

With the maximal possible vapor pressure drop, by taking $p_{\mathrm{L_T}} = 0$ at condenser endcap and $p_0 = p_\mathrm{sat}$ at evaporator endcap, the viscous limitation can be calculated. This assumption is made by Busse [12] and Faghri [10], it may hold for low saturation pressures or high temperature heat pipes going fast through this regime. But, for the investigated low temperature methanol heat pipes, the error for temperatures above −40 °C is significant. An alternative approach is presented by taking the liquid pressure drop additionally into account. Since the heat pipe is a closed system, the sum of the liquid and vapor pressure drop cannot exceed the maximal occurring pressure in the evaporator. At low temperatures, the maximal pressure drop is limited by the saturation pressure. As example for the temperature −40 °C at evaporator endcap and power 0.4 W the total pressure drop in liquid and in vapor is 200 Pa and the liquid friction part is 170 Pa. Saturation vapor pressure is as well 200 Pa. The viscous limitation is inhibiting the heat transfer as long as the saturation pressure p_sat is lower than the maximal capillary pressure drop $\Delta p_{\mathrm{c,max}}$. When the saturation pressure is higher than the maximal capillary pressure, the heat pipe is limited by the capillary pressure. Taking the liquid pressure drop into account, the viscous limitation can be described with

$$Q_{\mathrm{v,max}} = \frac{p_\mathrm{sat} H_\mathrm{fg}}{\left(\frac{\mu_\mathrm{l}}{\rho_\mathrm{l} A_\mathrm{w} K} + \frac{8\mu_\mathrm{v}}{\pi r_\mathrm{v}^4 \rho_\mathrm{v}}\right) L_\mathrm{Eff}}, \quad (3)$$

where the first term in the denominator describes the liquid pressure drop and the second describes the vapor pressure drop. This formulation is like that of the capillary limitation, but with the saturation pressure as reference.

The sonic limitation appears after the viscous limitation and is a thermodynamic barrier. In a heat pipe, the vapor flow may reach a Mach number of unity at the evaporator outlet or with an adiabatic section at the transition to the condenser section. Without this section, the flow reaches sonic velocity at the exit of the evaporator. This condition is reached when the heat pipe operates at high heat inputs or low saturation pressures. A similarity exists between a convergent-divergent nozzle and a heat pipe. Kemme [13] was the first noting this. In a convergent-divergent nozzle, the fluid flow can reach maximal a Mach number of unity at the throat. This is known as the choked flow condition. A heat pipe has no convergent section, the similarity origins from the mass addition at the evaporator. Analytical approximation of the sonic limitation can be made with the assumptions that the flow is a one-dimensional, compressible, frictionless, ideal gas. Three analytical approaches are made with the further assumptions, that the flow is isothermal, derived by Busse [12]; or that the flow is isentropic, derived by Levy [14]. The third attempt is made by Bertossi et al. considering the saturated vapor flow. This analysis takes the evolution of the thermophysical properties on the saturation curve, since they do not follow the ideal gas law [15]. Comparing the three approaches together, only low practical impact on the calculated sonic limitation can be found. In the analysis of this heat pipes, the vapor flow is investigated by CFD. It is found that for condenser temperatures below −60 °C sonic flow condition is reached at about −42 °C at the beginning of the evaporator. Lowering the condenser temperature does not affect the occurrence, due to the small variation of saturation pressure in the condenser. For a condenser temperature of −50 °C it is reached at −26 °C in the beginning of the evaporator, for −40 °C at −20 °C and for −30 °C at −9 °C, respectively. Above an operation temperature of −27±2 °C the heat pipe is dominated by the capillary limitation.

The capillary limitation is reached when the sum of the liquid and vapor pressure drop is higher than the maximal occurring capillary pressure. For a heat pipe with a metal fiber wick the maximal capillary pressure is defined by

$$p_{\mathrm{c,max}} = \frac{35\sigma}{d_f}(1-\varepsilon)\sqrt{1 - \exp\left(-\frac{6 d_f}{l_f}\right)} \quad (4)$$

with d_f and l_f as fiber diameter and length, respectively [16]. Taking the maximal capillary pressure from Eqn. 4 the hydrodynamic limitation can be described with

$$Q_{c,\mathrm{max}} = \frac{p_{\mathrm{c,max}} H_\mathrm{fg}}{\left(\frac{\mu_\mathrm{l}}{\rho_\mathrm{l} A_\mathrm{w} K} + \frac{8\mu_\mathrm{v}}{\pi r_\mathrm{v}^4 \rho_\mathrm{v}}\right) L_\mathrm{Eff}}. \quad (5)$$

This limitation dominates the operation of the heat pipe at temperatures above −27±2°C. The transition point at this temperature is defined by the condition $p_{\mathrm{c,max}} = p_\mathrm{sat}$. For $p_{\mathrm{c,max}} \geq p_\mathrm{sat}$, the

heat pipe is dominated by the viscous limitation and for $p_{c,max} \leq p_{sat}$ by the capillary.

The liquid and vapor are counter flows interacting together at the liquid-vapor interface. The shear stress causes the liquid to entrain the vapor flow. The liquid droplets are carried back toward the condenser section forming a liquid slug at the end cap. This phenomenon creates shortcut of the liquid return path, causing a faster dry-out at the evaporator accompanied by the capillary limitation. Kim et al. [17] [18] made experimental and mathematical analysis of the entrainment limit of a heat pipe with water as working fluid. In total, they found twelve different models predicting the occurrence of the entrainment limit. In their analysis they identified critical Weber numbers between 0.2 and 10. An expression of the entrainment limitation as made by Faghri [10] or Kim et al. [17], [18] does not provide an accurate estimation. A proper analytical descript of this limitation is impossible as all models predicting this limitation depend on empirically found parameters. Nevertheless, this limitation has its eligibility and must be considered as one limiting factor. In Fig. 4 the calculated heat transfer limitations for HP-A are shown (similar for HP-B).

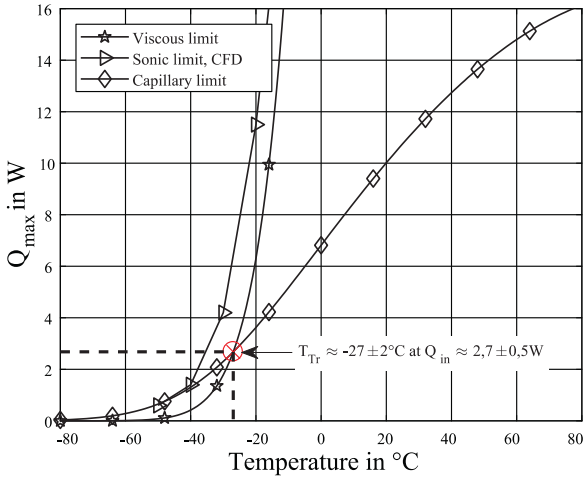

Fig. 4. Calculated heat transfer limitations of HP-A. HP-B is similar.

These are identified to be responsible for the variable conductance of MASCOT's heat pipes. At about -27±2 °C in the evaporator, a transition between the viscous to the capillary limitation happens. The sonic limitation is above the viscous limitation calculated with Eqn. 3. These two limitations are working together. For example, when a condenser temperature of -60 °C is the sonic limitation reached at an evaporator temperature of -42 °C. So, the heat pipe is at this point in choked flow conditions. But the maximal saturation pressure still dominates the heat transfer limitation since it is lower than the maximal capillary pressure until a temperature of -27±2 °C in the evaporator. Above this point is the heat pipe dominated by the capillary limitation.

3. EXPERIMENTAL SETUP

All tests were carried out at the DLR Bremen in a thermal vacuum chamber SSA (volume of 0.8m^3) in a pressure environment below 10^{-6} mbar, avoiding convective heat transfer. Fig. 5 shows the test set up inside the thermal vacuum chamber. The heat pipes (1) are fixated on the condenser block (2) and the evaporator stands (3).

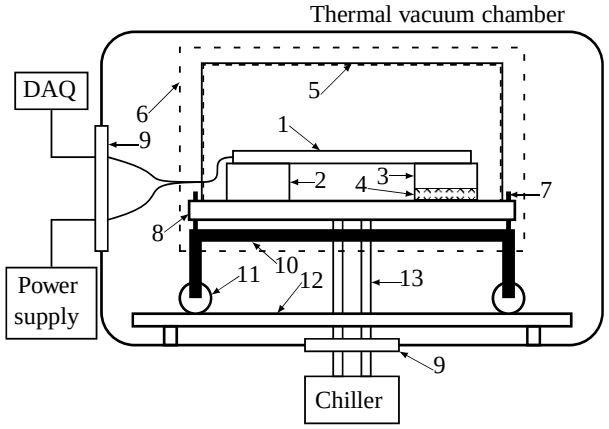

Fig. 5. General test setup in the thermal vacuum chamber. 1 – Heat pipe; 2 – Condenser block; 3 – Evaporator stand; 4 – Thermal insulation; 5 – Copper shroud with SLI cover; 6 – MLI cover around shroud; 7 – Alignment screws; 8 – Mounting plate (heat sink); 9 – Interfaces between thermal vacuum chamber and laboratory; 10 – Wagon (aluminum profile); 11 – Rolls; 12 – Rail; 13 – Cooling hose.

A thermal insulation (4) prevents heat transfer from the temperature support plate (8) to the evaporator. For a uniform temperature environment is a thermal compartment realized with a copper shroud (5) covering this plate. To have a uniform radiation inside the shroud, a single layer insulation (SLI) is attached on the inner walls. Outside, to minimize the temperature exchange, the mounting plate and shroud are covered with multi-layer insulation (MLI) (6). The plate stands on four alignment screws (7) on a wagon (10) made of aluminum profiles. They are used to align the mounting plate. Height difference between evaporator and condenser was measured with two Seika NBA3 inclination sensors (x and y tilt). Heat sink temperature (mounting plate) is regulated with a liquid cryostat Huber 385 (Chiller), and heaters are powered with power supply HAMEG HP4040.

The measurement system YOKOGAWA DC100 DAQ and twelve custom-made PT100 sensors with constantan wires records the temperature along the heat pipe shell (system accuracy of 0.05K). They are uniformly distributed in evaporator flange (4 units), adiabatic zone (4 units) and condenser zone (4 units). The power supply HAMEG HP4040 is remote controlled with LabVIEW for powering of heaters and recording of voltage, current and power values. The heating elements were operated in a constant voltage mode. The liquid thermostat and the DAQ were accessed via vendor software. SEIKA NBA3 inclination sensors and the power supply system were integrated in a LabVIEW environment to enable cross-communication and full automatic testing. Inside the DLR network the Windows tool “Remote desktop” was used to remote control of the testing computer. The access from outside was realized via Virtual Private Dialup Network (CISCO).

4. ACHIVEMENT OF VARIABLE CONDUCTANCE CHARACTERISTICS

A steady state test was conducted to get the regulative characteristics of the heat pipes. The sink is held at a constant temperature. The heat input is increased when steady state is reached in the evaporator (< 0.2 °C/h). The test is conducted for heat sink temperatures from −70 to 60 °C and heat inputs of 0.5 W to 16 W. Fig. 6 shows the change of the thermal resistance of HP-A. which is calculated by the dividing average temperature difference between evaporator and condenser by applied power. Both heat pipes show a change of thermal resistivity from about 70 K/W at a heat sink temperature of −70 °C, to 0.8 K/W at a heat sink temperature of +60 °C; with the maximal heat transfer rate of 5 W and 16 W, respectively.

Both heat pipes have in common, that below the found transition point of −27 °C no rise of resistance can be found, it decreases slightly approaching a constant value. When the heat sink temperature is above −20 °C, a first change of resistance can be found, for example for HP-A between 2 and 4 W. The first rise of the resistances is an indicator for reaching the capillary limitation. The deviation between calculated and measured limitation has different sources. First, the calculation of the maximal capillary pressure has an uncertainty of 15% [16]. It is found that for the capillary limitation the condenser temperature (approx.

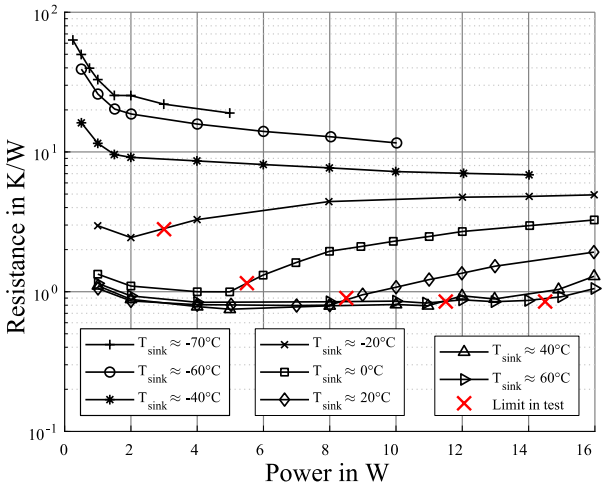

Fig. 6. Thermal resistance for HP-A for different heat sink temperature. Similar to that of HP-B. Resistance is calculated by the mean temperature difference between evaporator and condenser.

the same as heat sink temperature) is the best reference. For the viscous limitation, the evaporator temperature is the best reference, since this limitation is dependent on the maximal saturation pressure.

For temperatures above the transition point a sudden change in the resistance is observable. For temperatures below, it is not. The difference is in the change of condenser temperature. In the total heat pipe resistance, the resistance between adiabatic zone and the condenser dominant. The resistance between evaporator and adiabatic zone does not change significantly. This behavior can be explained by a formation of a liquid slug at the end of the condenser. The same test is conducted with a positive (condenser above evaporator) and a negative (condenser below evaporator) inclined heat pipe. The observation for the negative inclined heat pipe reinforces this explanation.

5. RESULTS OF THERMAL CYCLING AND START-UP TESTS

During the thermal cycling test, the power input is hold constant and the sink temperature is suddenly lowered. The transient behavior is now examined, to identify the transition point from nearly adiabatic to non-adiabatic working point (capillary limitation). This switching effect is a desirable feature to separate the evaporator from the condenser. Fig. 7 shows an example of a temperature cycle from 60 °C to −60 °C for HP-A.

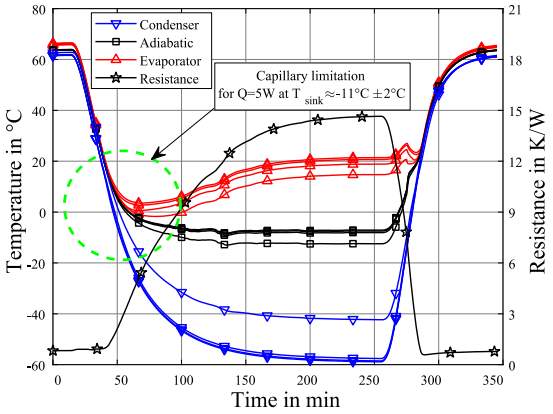

Fig. 7. Thermal cycling of HP-A at a constant heat input of 5W from 60°C to −60°C and change of resistance/conductivity during sink cooling. Similar behavior for HP-B observed.

The acting limitation is the capillary. For a heat input of 5 W, it is calculated to be at a sink temperature of about 11°C. Additionally the change of resistance during the cycle is shown. At about 40 minutes the resistance begins to rise, at this point the heat pipe encounters the capillary heat transfer limit. The limiting sink temperature is identified in the test at about 5 °C. CFD analysis for this case shows, that the maximal velocity is at about M = 0.35. The beginning of the switching effect is therefore not the sonic limitation. After this point, the temperature drops further causing a higher pressure difference. When this difference is high enough, the sonic limitation finally separates the condenser due to chocked condition. This is indicated by a constant temperature at the end of the adiabatic section. While the temperature in the condenser drops further, which is the typical behavior for this limitation. Additional test with a heat input of 10W shows that the switching effect occurs near the calculated capillary limitation ($T_{\mathrm{sink}} \approx 20$ °C at $Q_{\mathrm{in}} = 10$ W). This indicates that the capillary limitation is the cause of the first transition point. Another phenomenon can be observed at about 65 minutes, the evaporator begins to dry-out indicate by the rise temperature. This dry-out benefits the formation of a liquid slug at the end of the condenser. In additional cycles from 20 to −40 °C and 20 to −10 °C with same heat input, the heat pipes show the same transition point as in Fig. 7, indicating that the switching point occurs at the same sink temperature and does not depend on the maximal cooling temperature. The heat pipes repeated their characteristics after being in essential overheating 20…40 °C in the evaporator.

At cycling between −20 °C and −70 °C with applied power 1 W two main differences with Fig. 7 are observed. First the heat pipe does not encounter the capillary limitation and is in the viscous regime. The heat input is below the calculated transition power between viscous and capillary limitation of 2.7±0.5 W (Fig. 4). Because the capillary limitation is not encountered, the governing temperature reference is at the evaporator. The switching effect is now at the transition temperature of about −27±2 °C in the evaporator beginning. And second, the temperature profile is different. The temperature in the adiabatic section is not uniform but drops linear from evaporator to condenser. CFD analysis for a sink temperature of −70 °C shows, that a temperature of −42 °C at beginning of evaporator is required to reach sonic limitation. The evaporator temperature at steady-state is at about −34 °C, which means that the heat pipe is in sonic limitation. But the temperature in the adiabatic section drops further contrary to the theory, this can be an effect of thermal conduction trough the shell and wick of the heat pipe. The information of a colder condenser may not propagate backwards trough the sonic vapor flow, but trough the wick and shell. It seems that the heat transfer trough the vapor with low density is not high enough to keep a constant adiabatic temperature, as it is the case for higher heat inputs. In conclusion of the thermal cycling test can be said, that the heat pipes are governed by the capillary limitation at high heat inputs. This limitation is the only one which determines the first transition point from adiabatic to non-adiabatic working condition. At lower heat inputs, the temperature drops further reaching the viscous limitation. This limitation is the only which defines the second transition point at low temperatures / heat inputs.

To verify the second transition point ($p_{\mathrm{sat}} = p_{\mathrm{c,max}}$ at −27±2 °C) various start up tests were made. During this test period is the sink temperature hold constant and a sudden heat input above the calculated limitations is applied. The evolution of the temperature in the evaporator gives hints in the occurrence of heat transfer limitations. While at the thermal cycling test, the capillary limitation is first encountered for high heat inputs, it is the opposite for startup test. Because the heat pipes start at low temperatures, they go first through the viscous and sonic regime reaching the capillary limitation. In Fig. 8 is the start at a sink temperature −60 °C with a heat input of 5 W shown. The transition point between the capillary and viscous limitation is found to be at the calculated temperature.

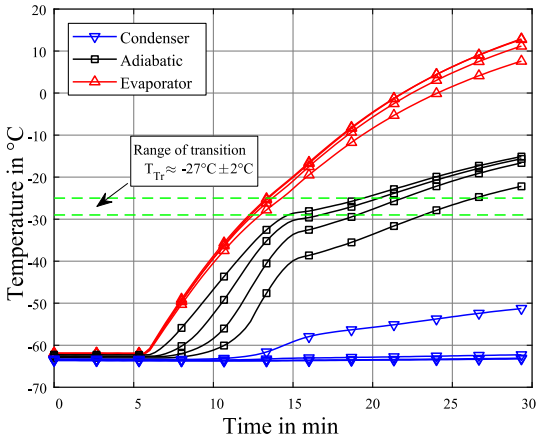

Fig. 8. Start at a sink temperature of -60°C and heat input of 5W for HP-A.

When the evaporator reaches this transition point, the temperature profile changes along the heat pipe. A dry-out in the evaporator is indicated by the high temperature drop to the adiabatic section. In the adiabatic section the temperature becomes uniform and in the condenser the formation of the liquid slug is visible due to the rise at the entrance and the constant temperature in the rest of it. The occurrence of the transition point is not depended on the heat input nor on the sink temperature. It solely depends on the fact if the temperature in the beginning of the evaporator is at about −27 °C or not. The occurrence was tested for sink temperatures of −75 °C, −70 °C, −60 °C and −40°C and for heat inputs of 5W, 10W and 15W. While this effect is good visible for sink temperatures up to -60 °C, it is indistinctly for a sink temperature of −40 °C. The reason is the exponential nature of the saturation pressure of methanol. In conclusion of the startup tests can be said, that the saturation and the maximal capillary pressure determines the point at low temperatures, where the heat pipe switches and changes its temperature profile. During the heating, the heat pipes goes also trough the sonic limitation. It is obvious, that these phenomena cannot be described with the viscous limitation as given in literature (Eqn. 2). In the derivation of this limitation are the inertia forces neglected, but the test shows, that this point is even reached when sonic vapor flow is present. This limitation is a rather a second pressure-based limit, as like the capillary limitation (Eqn. 3) and not the classical viscous limitation as described by Busse [12].

To verify the transition point hypothesis for $p_{\mathrm{sat}} = p_{\mathrm{c,max}}$ is an additional test with an inclined heat pipe performed. The inclination benefits the liquid flowback to the evaporator. This ensures that the capillary limit is raised due to gravity assist. A higher maximal capillary pressure moves the transition point to higher temperatures. The new calculated transition point is at about -22±2 °C and is confirmed by the inclined heat pipe test.

This indicates that the hypothesis is correct and that another influence on the occurrence of this transition point can be excluded. The dry-out in the evaporator is also not as distinct as for the non-inclined heat pipe due to the beneficial flow back of working fluid to the evaporator.

6. HEAT PIPE OPERATION WITH HEAT OUTPUT BY RADIATION

In the course of MASCOT TCS R&D activity the heat pipes operation were verified in one thermal vacuum test on subsystem level and six thermal vacuum tests on system level.

The start-up from cold initial temperature with largest applied heat power had most concerns. Heat pipe start from initial temperature −20 °C in evaporator and −85 °C in condenser with uncooled condensation zone and applied power 10 W is performed in [9]. It has shown the essential rise of the evaporator temperature till 80 °C with temperature difference along heat pipe in 120 °C. After condenser and vapor temperature reaches −40 °C and 20 °C for HP-A (0 °C and 10 °C for HP-B), normal evaporation–condensation cycle started and evaporator temperature decreased to 40 °C. No comment on HP behavior is presented [9].

Considering an importance of such starting regimes at low initial temperature, the thermal mock-up of TCS system was designed (Fig. 9). It consists of an imitator of electronic box heat supply (heater 1), two heat transferring flanges, two heat pipes (HP-A and HP-B), an aluminum honeycomb radiator, mechanical supports and a thermal shroud.

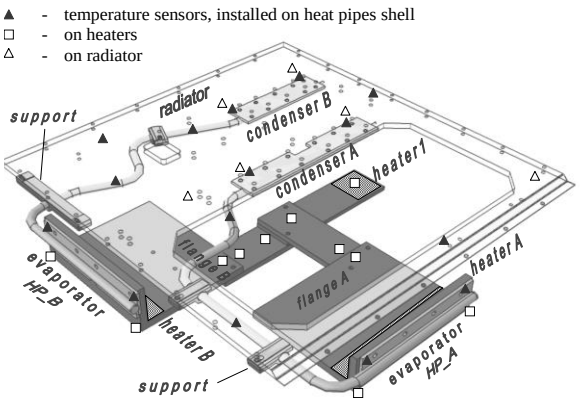

Fig. 9. Scheme of thermal mock-up of TCS for autonomies test of MASCOT 2D heat pipes. Protection shrouds, MLI, montage plate are not shown.

Previously described 2D configured heat pipes were used, transferring heat from the imitator of electronic box (heater 1) to radiator. Individual heaters A and B, installed on corresponding flanges are used for individual test of heat pipes. The test assembly was placed on a horizontal plane. Mechanical supports were used to hold heat pipes in a horizontal plane as they have individual deviation in shape.

The test run can be divided into four parts (Fig. 10). In part A, there is temperature stabilization at low heat transfer Q = 0.8 W. Part B is a preheating phase with a heater power of Q = 5.0 W. In part C and D, electronic box operation is simulated by a heat input of 9.3 W for each heat pipe. Temperature difference between the evaporator and the condenser is 32 °C in part A and 11 °C in part D, although the applied heater powers differ eleven times. Variation of heat pipe thermal resistance reaches the value 40:1.1. No overheating of heater has been observed. Different character of startup [9] and current test is connected with the impact of heat capacity ratio $\varphi = C_{ev} / (C_{con} + C_{rad})$ on evaporator overheating over steady state value. At condition of current experiment at value $\varphi > 2$ the overheating is not observed, at $\varphi < 1$ it reaches 5 °C and more.

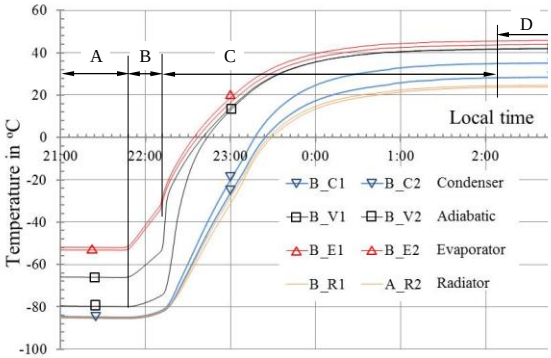

Fig.10. HP-B startup from cold conditions: H –heater, E- evaporator, V- adiabatic, C - condenser, R –radiator.

The thermal vacuum tests (TVAC) on a system level. TCS work as part of MASCOT lander. The following phases are important: heat pipe operation in cruise with minimal applied power and lowest external fluxes on radiator (Fig. 11). Radiator lays on temperature level −70…−40 °C, heat pipe blocks the heat transfer from electronic block to radiator, providing minimal power consumption from HY2. After preheating the initiating of MASCOT electronic is foreseen.

Heat pipe thermal resistance in cruise hibernation is larger than 20 K/W (at T_{rad} = −65 °C), rising to value higher than 6 K/W in preheating phase.

In experimental simulation of MASCOT operation on asteroid surface three variable values act on TCS: inner power generation; asteroid soil temperature and an illumination of lander sides, and main radiator (Fig. 12).

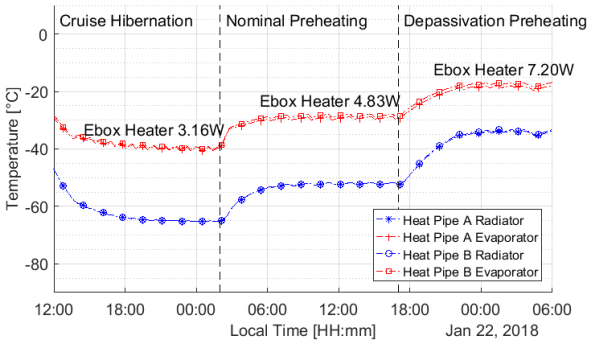

Fig. 11. Heat pipes operation in TVAC in cruise (hibernation and preheating).

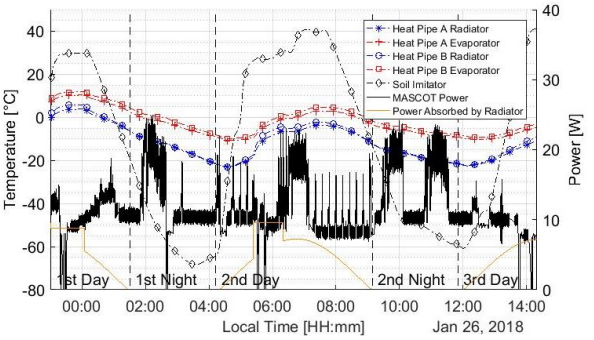

Fig. 12. Heat pipes temperatures in TVAC during on asteroid soil operation (one of the nominal cases).

Heat pipe thermal resistance is about 1.2 and 4 K/W at sun illuminated period and during night correspondently. Temperature of evaporator lies inside −10…+5 °C, which provides the acceptable temperature conditions for lander electronics.

Flight performance. After the HY2 spacecraft launch, 11 sets of telemetric contacts took place. Heat pipe system has repetitively confirmed the ability to start from the high thermal resistance condition to the low one. Preparation of MASCOT lander to separation from spacecraft and landing on asteroid is going till middle of 2018.

7. CONCLUSIONS

Methanol-copper heat pipes with a fibrous capillary copper structure are characterized as a part of the MASCOT lander TCS. They have shown a change of their thermal resistance by two orders, as a function of the applied heat flux (0.25…10 W) and heat sink temperature (−70…+60 °C). Performed study shows that such variable properties are the sequence of inner heat transfer process changes, taking place at passing the vapor sonic velocity limit, viscous limit and the capillary limit. A transition

point for the condition $\Delta p_{c,max} = p_{sat}$ is found to be at about 27±2 °C in the evaporator. Below this point the heat pipes are in viscous limitation showing nearly linear temperature drop in the adiabatic zone and constant temperatures in the evaporator and condenser. For temperatures above the transition point the heat pipes are in capillary limitation with typical dry-out phenomena in the evaporator shown by a temperature drop between evaporator and adiabatic zone. After being in overheated conditions with temperature difference between evaporator and condenser of 110 °C, the heat pipes return in normal mode of operation as typical for conventional heat pipes. Heat pipes operation in the TCS of MASCOT lander, observed in ground thermal vacuum tests and in flight during 2014-2017, did not show deviations from expected performance of thermal control system.

NOMENCLATURE

A_v : Vapor cross area (m^2)
A_w : Wick cross area (m^2)
C : Heat capacity (J/K)
d_s : Outer heat pipe diameter (m)
d_v : Vapor space diameter (m)
d_w : Inner heat pipe diameter (m)
H_{fg} : Heat of vaporization (J/kg)
K : Wick permeability (m^2)
L_A : Adiabatic zone length (m)
L_C : Condenser zone length (m)
L_E : Evaporator zone length (m)
L_{Eff} : Effective heat pipe length (m)
L_T : Total heat pipe length (m)
m_{HP} : Mass heat pipe (kg)
p_{sat} : Saturation pressure (N/m^2)
V_{wf} : Volume working fluid (ml)
ε : Wick porosity (—)
λ : Thermal conductivity (W/(mK))
μ : Viscosity (Pa s)
ρ : Density (kg/m^3)
σ : Surface tension (N/m)

REFERENCES

[1] Watanabe S. et al., Hayabusa2 Mission Overview. *Springer, Astronomy Highlights 2017, Space Science Reviews*, July 2017, Volume 208, Issue 1-4, pp. 3–16.

[2] Jaumann R. et al., The Camera of the MASCOT Asteroid Lander on Board Hayabusa 2. *Springer, Astronomy Highlights 2017, Space Science Reviews*, July 2017, Volume 208, Issue 1-4, pp.375-400.

[3] Bibring J.P. et al., The MicrOmega Investigation Onboard Hayabusa2. *Springer, Astronomy Highlights 2017, Space Science Reviews*, July 2017, Volume 208, Issue 1-4, pp. 401-412.

[4] Hercik D. et al., The MASCOT Magnetometer. *Springer, Astronomy Highlights 2017, Space Science Reviews*, July 2017, Volume 208, Issue 1-4, pp. 433-449.

[5] Grott M. et al., The MASCOT Radiometer MARA for the Hayabusa 2 Mission. *Springer, Astronomy High-lights 2017, Space Science Reviews*, July 2017, Volume 208, Issue 1-4, pp. 412-431.

[6] Celotti L. et al., Mascot thermal subsystem design challenges and solution for contrasting requirements. *45th Int Conference on Environmental systems*, 12-16 July, 2015, Washington, USA. Report ICES-2015-83.

[7] Baturkin V., Zhuik S., Savina V., Development and research of heat pipes for thermal control system of scientific apparatus .*IV international seminar, 18-24 September, 1989*, t. Frunze, USSR, Institute of space research, USSR Academy of sciences, 1990., pp. 201-208.

[8] Baturkin V. et al. Elaboration of thermal control systems on heat pipes for microsatellites Magion 4, 5 and BIRD. *Applied Thermal Engineering*. 2003, Vol.23, pp. 1109-1117.

[9] Kravets V. et al., Heat pipes with variable thermal conductance property developed for space applications. *Journal of Mechanical Science and Technology*, 31(6), 2016, pp. 2613-2620

[10] Amir Faghri, *Heat Pipe Science and Technology*, Global Digital Print, 2016.

[11] Semena M., Method of computing the thermal resistance of low-temperature heat pipes with metal-fiber wicks, *Journal of Engineering Physics*, Bd. 36, Nr. 3, 1979, pp. 287–292.

[12] Busse C.A., Theory of the ultimate heat transfer limit of cylindrical heat pipes. *International Journal of Heat and Mass Transfer*, Bd. 16, Nr. 1, pp. 169 186, 1973.

[13] Kemme J.E. Ultimate heat-pipe performance. *IEEE Transactions on Electron Devices*, Bd. 16, Nr. 8, pp. 717–723, 1969.

[14] Levy E. K., Theoretical Investigation of Heat Pipes Operating at Low Vapor Pressures, *Journal of Engineering for Industry*, Bd. 90, Nr. 4, pp. 547, 1968.

[15] Bertossi R. et al., THEORETICAL STUDY AND REVIEW ON THE OPERATIONAL LIMITATIONS DUE TO VAPOUR FLOW IN HEAT PIPES, *Frontiers in Heat Pipes*, Bd. 3, Nr. 2, 2012.

[16] Semena M., Gershuni A., Analysis of the capillary-transport characteristics of metal-fiber structures, *Journal of Engineering Physics*, Bd. 1981, Nr. 41, pp. 683–688.

[17]. Kim B. H., Peterson G. P., Analysis of the critical Weber number at the onset of liquid entrainment in capillary-driven heat pipes, *International Journal of Heat and Mass Transfer*, Bd. 38, Nr. 8, pp. 1427–1442, 1995.

[18] Kim B. H., Peterson G. P., Theoretical and physical interpretation of entrainment phenomenon in capillary-driven heat pipes using hydrodynamic instability theories, *International Journal of Heat and Mass Transfer*, Bd. 37, Nr. 17, pp. 2647–2660, 1994.